remote sensing

MDPI

Article

Girth-Based Anchor Matching for Handheld SLAM LiDAR Forest Inventory Under Closed Tropical Canopies

Naruemol Kaewjampa [1], Piyapong Tongdeenok [1], Renuka Klabsuk [1], Surachit Waengsothorn [2], Hyeon Tae Kim [3] and Sitthisak Moukomla [4,*]

[1] Department of Conservation, Faculty of Forestry, Kasetsart University, Bangkok 10900, Thailand; ffornmk@ku.ac.th (N.K.); piyapong.t@ku.th (P.T.); renuka.k@ku.th (R.K.)
[2] Sakaerat Environmental Research Station, Thailand Institute of Science and Technological Research, Nakhon Ratchasima 30370, Thailand; surachit@tistr.or.th
[3] Department of Bio-Systems Engineering, Institute of Smart Space Agriculture (ISSA), Gyeongsang National University, Jinju 52828, Republic of Korea; bioani@gnu.ac.kr
[4] Research Unit in Geospatial Research and Analytics for Climate and Environment and Department of Geography, Faculty of Liberal Arts, Thammasat University, Khlong Luang District, Pathum Thani 12120, Thailand
* Correspondence: moukomla@tu.ac.th

Highlights

What are the main findings?

- A few trees marked with ordinary reflective tape are enough to align an entire dense tropical plot, so every other tree can then be linked to the field inventory by its girth alone—no per-tree GNSS needed.
- The very reflective tape is automatically picked up by the SLAM scanner's intensity channel, so the anchors that align the plot can also be detected without any manual mark-up.

What are the implications of the main findings?

- Closed-canopy forests that were previously too dense for GNSS-based mobile-LiDAR inventory can now be mapped in under an hour by a single person walking with a handheld scanner.
- The workflow is affordable for tropical national forest inventories and repeat carbon-MRV surveys where high-grade GNSS receivers are out of reach.

Abstract

Per-tree geolocation in closed tropical canopies has typical uncertainties of 5–15 m with GNSS receivers, preventing automated linking of field inventories to point-cloud stem data. We propose an anchor-based matching framework that does not require per-tree GNSS. A handheld SLAM LiDAR scanner maps stems and girths within ≈40 min; field crews record species, girth, and serial numbers without physical markers or tools. Dataset linkage uses a small subset of reflective-tape anchor trees (35 and 43 per hectare, roughly one per 400–500 m^2) with approximate GNSS locations. Species identity is transferred using median-based GNSS bias correction and quadrant-partitioned Hungarian matching with global deduplication; accuracy is validated by leave-one-anchor-out (LOAO) tests and exact binomial statistics. Tested in two 1-ha plots of open Dry Dipterocarp Forest (DDF; 280 trees/ha) and dense Dry Evergreen Forest (DEF; ~1054 trees/ha) at the Sakaerat Biosphere Reserve, Thailand, SLAM girth matched tape data with R^2 = 0.997, RMSE = 1.82 cm in DDF; in DEF, after correcting a 6.38 m GNSS bias, R^2 = 0.986 and RMSE = 7.01 cm, with ≥99% detection for stems ≥30 cm girth (99.2% DDF; 100% DEF). LOAO accuracy

Check for updates

Received: 22 April 2026
Revised: 25 May 2026
Accepted: 9 June 2026
Published: 10 June 2026

Copyright: © 2026 by the authors. Licensee MDPI, Basel, Switzerland. This article is an open access article distributed under the terms and conditions of the Creative Commons Attribution (CC BY) license.

was 35/35 in DDF and 40/43 in DEF. Retroreflective-tape anchors were additionally detected automatically from the SLAM intensity channel in 71.4% of DDF anchors (95% CI 53.7–85.4) and 76.7% of DEF anchors (95% CI 61.4–88.2) at intensity $\geq$ 150 DN, with up to 59-fold enrichment over matched non-anchor controls at I $\geq$ 250 in DEF (Fisher's exact $p < 1 \times 10^{-15}$), enabling a fully automated anchor-detection pipeline.

Keywords: SLAM LiDAR; tropical forest inventory; GNSS-denied matching; Hungarian algorithm; anchor-based registration; girth estimation

1. Introduction

Individual-tree measurements, namely species, stem diameter and more recently height from permanent sample plots, are needed for national forest inventories [1] and for REDD+ verification programs [2]. As a result, collecting these inventory data remains expensive in tropical forests: for example, one trained crew usually requires 3–5 person-days to survey one hectare of dense forest. The most time-consuming and limiting step for this work is not the identification of species (which requires nontrivial botanical knowledge), but the component of measuring hundreds to thousands of stems across a plot. One clear improvement would be giving each tree a GNSS position so they could all be automatically linked to remote-sensing products. In reality, this does not work beneath tropical canopies. Dual-frequency RTK receivers drop to meter-level accuracy under closed forest [3,4] and can exceed 5–15 m in multi-layered evergreen stands [5]. Automated identity assignment becomes impossible because at that error level all candidate trees fall inside any positioning circle. The most important forests to monitor—structurally complex tropical systems that contain a disproportionate share of terrestrial carbon [6,7]—are also the ones with the greatest uncertainty associated with individual tree geolocation.

A partial escape is offered by hand-held SLAM (Simultaneous Localization and Mapping) LiDAR. Scanners such as the GeoSLAM ZEB series, Leica BLK2GO and GVI LiGrip weigh less than 2 kg and produce dense 3D point clouds as an operator walks through the forest [8–10]. Such systems attain DBH accuracies of 1–3 cm in European and boreal forests [8,11,12]. SLAM therefore solves the measurement-speed problem but not the identity problem. A SLAM point cloud contains geometrically positioned stems rather than named trees; linking them back to field-identified species has traditionally required per-tree GNSS. Existing studies have approached the matching step through two unsatisfactory routes. One is manual matching, where an expert compares visually point-cloud stems with the inventory map [13,14]. This approach is subjective, non-reproducible, and scales poorly to thousands of stems. The second is nearest neighbor assignment from GNSS locations [15,16], which performs adequately when the GNSS error remains below the mean inter-tree distance (<~3 m) but fails catastrophically otherwise—a condition that in a closed tropical forest is usually the norm [10,17]. Nearest-neighbor assignment fails far more readily in dense tropical forests than in temperate or boreal stands: stem densities are several times higher, so many candidate stems fall within any plausible search radius, and the 5–10 m GNSS error under closed canopy routinely exceeds the mean inter-stem spacing, so the true stem is seldom the nearest one.

Here we test a framework that eliminates per-tree geolocation entirely. Rather than recording a GNSS fix for every stem, we selected a small set (35 and 43 per hectare, roughly one per 400–500 m^2) as anchor trees, marked with ECE R-104 Class C micro-prismatic PET retroreflective tape wrapped once at breast height (~1.3 m); the retroreflective coating makes these anchors readily identifiable both visually in the understory and in the SLAM intensity

channel, where returns at the tape surface approach the sensor's 8-bit ceiling while bark returns remain in the low tens of DN. The approximate GNSS coordinates and measured girths of these anchors provide a sparse yet sufficiently constrained spatial framework to estimate and correct the systematic GNSS–SLAM coordinate offset. Once this bias is removed, the remaining hundreds of stems are matched automatically using a quadrant-partitioned optimal-assignment procedure based on the Hungarian algorithm [18,19], with a distance cost matrix and a forced one-to-one global deduplication step. We evaluate this anchor-based framework in two 1-ha permanent plots that span the structural extremes of a tropical gradient at the Sakaerat Biosphere Reserve, Thailand: a Dry Dipterocarp Forest (DDF; open canopy, 280 trees ha^{-1}) and a Dry Evergreen Forest (DEF; closed, multilayered canopy, ~1054 trees ha^{-1}). We address three questions: (1) Can handheld SLAM measure girth with accuracy comparable to conventional field methods used in tropical forests? (2) Is a sparse anchor network sufficient to bridge the GNSS gap and enable reliable automated matching under canopy-induced biases >6 m? (3) How does forest structural complexity affect measurement accuracy and matching performance?

Specifically, these are (i) a fully automated, mathematically specified anchor-based matching framework that requires no per-tree GNSS and is tolerant to extreme canopy-induced GNSS degradation; (ii) the first quantitative assessment of handheld SLAM girth estimates in a tall tropical evergreen forest with stem density >1000 ha^{-1}; (iii) empirical proof that just 35–43 anchors per hectare (≈4% of stems in the dense evergreen forest, and a higher fraction in the sparser deciduous forest) are sufficient for correcting biases up to 6.4 m and achieving ≥99% detection of carbon-relevant stems (≥30 cm girth; 99.2% DDF, 100% DEF), cross-validated through leave-one-anchor-out validation; (iv) a practical field protocol reducing per-hectare inventory time from 3 to 5 person-days to ∼1 person-day; and (v) quantitative evidence that ECE R-104 Class C retroreflective tape produces a LiDAR intensity signature statistically separable from bark returns (Fisher's exact $p < 1 \times 10^{-15}$ at $I \geq 150$ in DEF), opening a path to fully automated anchor detection without visual searching.

2. Materials and Methods

2.1. Study Area

The Sakaerat Environmental Research Station (SERS; 14°31′N, 101°56′E) is situated in approximately 80 km^2 of protected forest along the western fringe of the Khorat Plateau, Nakhon Ratchasima Province, north-eastern Thailand (Figure 1).

Since 1967, the site has facilitated ongoing assessments of ecosystem response (e.g., eddy-covariance flux tower and permanent plots). Climate: mean annual rainfall is ~1200 mm, concentrated in a wet season (May–October) characteristic of the Southeast Asian monsoon; mean annual temperature is 26 °C. Two 1-ha permanent plots (100 m × 100 m) were selected to span the structural range of the reserve (Table 1).

Dry Dipterocarp Forest (DDF) plot is fire-maintained open woodland on shallow sandy-lateritic soils dominated (by basal area) by the tree species *Shorea obtusa*, *S. siamensis*, *Dipterocarpus obtusifolius* and *D. tuberculatus*. Canopy cover is 40–60%, canopy height 15–25 m, and stem density 280 trees ha^{-1} (girth ≥ 15 cm at 1.3 m); the understory is dominated by C_4 grasses and herbs, with low liana load and nearly absent buttresses. The DEF plot supports a species-rich, multi-layered stand on deeper loamy soil (300–600 mm depth over alluvial clay), comprising 37 canopy-tree species; emergent of *Hopea ferrea* and *Dipterocarpus alatus* reach 35–45 m, with stem density ~1054 ha^{-1}. Point-cloud-based girth estimation in the DEF is complicated by two structural features: ≈18% of large stems (>60 cm girth) carry basal buttresses, and woody-liana incidence on these stems reaches ≈40%. GNSS reception is systematically degraded under the DEF canopy (positioning

errors 5–10+ m), offering a challenging natural experiment for the proposed framework. Table 2 shows the composition of basal area (m^2 ha^{-1}) for the top 10 species in each plot.

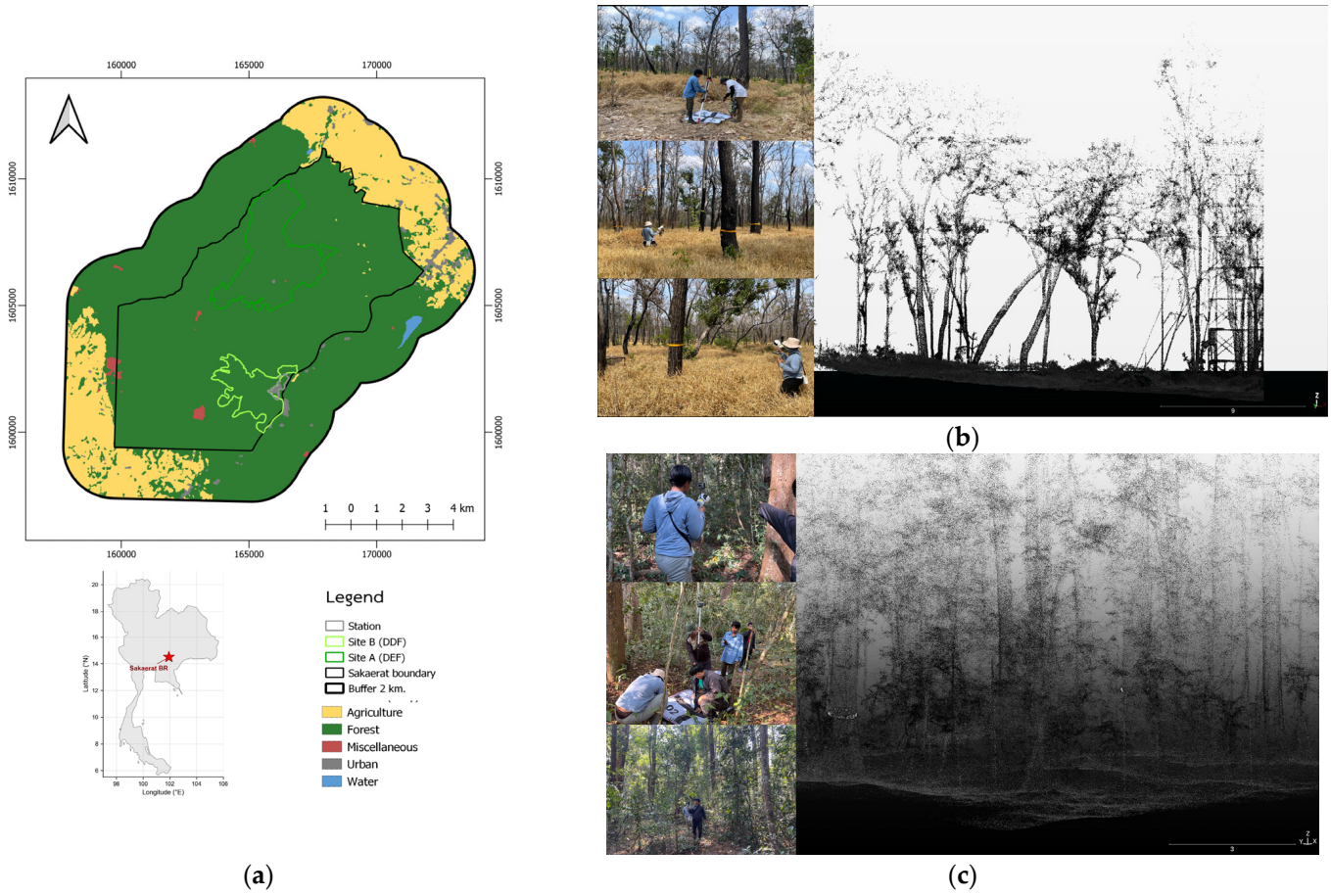


Figure 1. Study-site overview. (**a**) Regional location of the Sakaerat Environmental Research Station (SERS) in Nakhon Ratchasima Province, north-eastern Thailand; (**b**) DDF plot with the 35 field anchors overlaid on the SLAM-derived stem map; anchors span all four quadrants and the full 15–250 cm girth range. (**c**) DEF plot with the 43 field anchors; note the denser stem field and closed-canopy conditions that motivate the girth-based matching strategy.

Table 1. Study site characteristics of the two permanent plots at Sakaerat Biosphere Reserve.

Attribute	DDF	DEF
Forest type	Dry Dipterocarp	Dry Evergreen
Dominant species	*Shorea obtusa*, *S. siamensis*	*Hopea ferrea*, *Dipterocarpus alatus*
Canopy cover (%)	40–60	>90
Canopy height (m)	15–25	35–45
Stem density (trees ha^{-1})	~280	~1054
Field-measured trees	266	1054
Anchor trees (reflective tape)	35	43
Buttressed stems (>60 cm girth)	≈1%	≈18%
Woody-liana incidence (large stems)	<5%	≈40%

Table 2. Top 10 species by basal area in DDF and DEF plots.

#	DDF—Species	% BA	DEF—Species	% BA
1	*Shorea obtusa*	28.4	*Hopea ferrea*	14.8
2	*Shorea siamensis*	21.6	*Dipterocarpus alatus*	11.2
3	*Dipterocarpus obtusifolius*	15.1	*Syzygium cumini*	7.6
4	*Dipterocarpus tuberculatus*	10.7	*Hydnocarpus ilicifolius*	6.3
5	*Xylia xylocarpa*	5.9	*Aglaia lawii*	5.8
6	*Terminalia mucronata*	3.8	*Memecylon edule*	4.9
7	*Pterocarpus macrocarpus*	3.2	*Mitragyna hirsuta*	4.5
8	*Gluta usitata*	2.6	*Garcinia cowa*	4.1
9	*Irvingia malayana*	2.2	*Cinnamomum iners*	3.7
10	*Buchanania lanzan*	1.7	*Xylopia pierrei*	3.2
	Subtotal	95.2	Subtotal	66.1
	Other	4.8	Other (27 spp.)	33.9

2.2. Data Acquisition

2.2.1. Handheld SLAM LiDAR

We used a handheld SLAM LiDAR device—specifically, the LiGripH120 (hardware revision A.10 from Green Valley International in Beijing). It captures up to 320,000 points every second, with a maximum range of 120 meters and an impressive ±1 cm accuracy. The sensor offers a wide view, with 280° vertically and a full 360° horizontally, all while weighing just 1.83 kg, making it surprisingly portable for detailed scanning work. The data were collected in PPK-SLAM mode, with the scanner collecting LiDAR returns and raw GNSS observations simultaneously and a nearby CORS base station applied post hoc differential corrections to yield absolute accuracy $\leq$5 cm and relative accuracy $\leq$ 1 cm (per vendor specifications) using LiDAR360. LiDAR360 reported the SLAM trajectory loop-closure residuals as 3.2 cm (DDF) and 4.7 cm (DEF), which are both acceptable bounds for plot-scale inventory. All plots were walked in a meandering fashion at ~0.5–1.0 m s^{-1}, taking approximately 40 min to cover one hectare. The point clouds were exported as LAS files in UTM Zone 47N (WGS 84), with DDF containing $\sim 15 \times 10^6$ points and DEF $\sim 25 \times 10^6$.

2.2.2. UAV LiDAR (Auxiliary Data)

Canopy-level data was acquired with a DJI Matrice 300 RTK quadcopter (SZ DJI Technology, Shenzhen, China) carrying a CHCNAV AlphaAir 450 LiDAR system (CHC Navigation, Shanghai, China), which integrates a Livox Avia non-repetitive scanner (Livox Technology, Shenzhen, China) delivering up to 720,000 points per second in triple-return mode. Flights were conducted at 60–80 m above ground level (AGL) with 30–50% side lap between adjacent flight lines. A DTM and DSM were produced by standard ground-filtering of the point cloud, and a CHM was derived as DSM − DTM. This study's UAV data was only used to visually inspect and cross-reference tree plot extents; fusion of height data is reserved for a companion paper.

2.2.3. Field Inventory

All stems with girth $\geq$ 15 cm at breast height (h = 1.3 m) were measured with a diameter tape, labeled to assist in identification and assigned a unique serial number, beginning from 1 on the day of plot demarcation. The 15 cm girth threshold (≈4.8 cm DBH) was intentionally selected as a more sensitive value than the standard tropical DBH $\geq$10 cm cut-off, such that this paper measures the low end of the sensitivity of the sensor in dense understory; biomass analyses downstream are restricted to standard girth $\geq$30 cm

(≈9.5 cm DBH). For buttressed stems, girth was taken at the lowest point above the buttress following Condit (1998) [20]. Measurements followed a standardized serpentine order matching the SLAM traversal; per-tree GNSS coordinates were deliberately not recorded. 35 trees (DDF) and 43 trees (DEF) were selected as anchors by aiming to (i) cover the full girth range in 5 equal-frequency bins, (ii) sample evenly across space (one per 400–500 m^2 cell of a 5 × 5 grid), and (iii) be visually distinctive from surrounding trees. We marked the position of each anchor with ECE R-104 Class C micro-prismatic PET retroreflective tape (approximately 50 mm wide, single-wrap at breast height, ~1.3 m above local ground), and recorded its approximate location with a handheld GNSS (expected error 2–10 m under canopy); set-up took ~45 min per plot. The dry-dipterocarp and dry-evergreen surveys were acquired during a single field campaign during 2–6 February 2026, with the SLAM scan and field inventory of each plot completed together. Anchors were chosen to give an even spatial spread, which stabilizes the quadrant partition, and to span the full girth range, so that the girth-similarity gate is exercised across all size classes.

2.3. SLAM Point Cloud Processing

The processing pipeline converts a raw SLAM point cloud to a minimally georeferenced list of stem positions and girths in four steps (Figure 2). Core Libraries: all algorithms were implemented in Python (version 3.12.13) using NumPy, SciPy, scikit-learn (DBSCAN), and laspy.

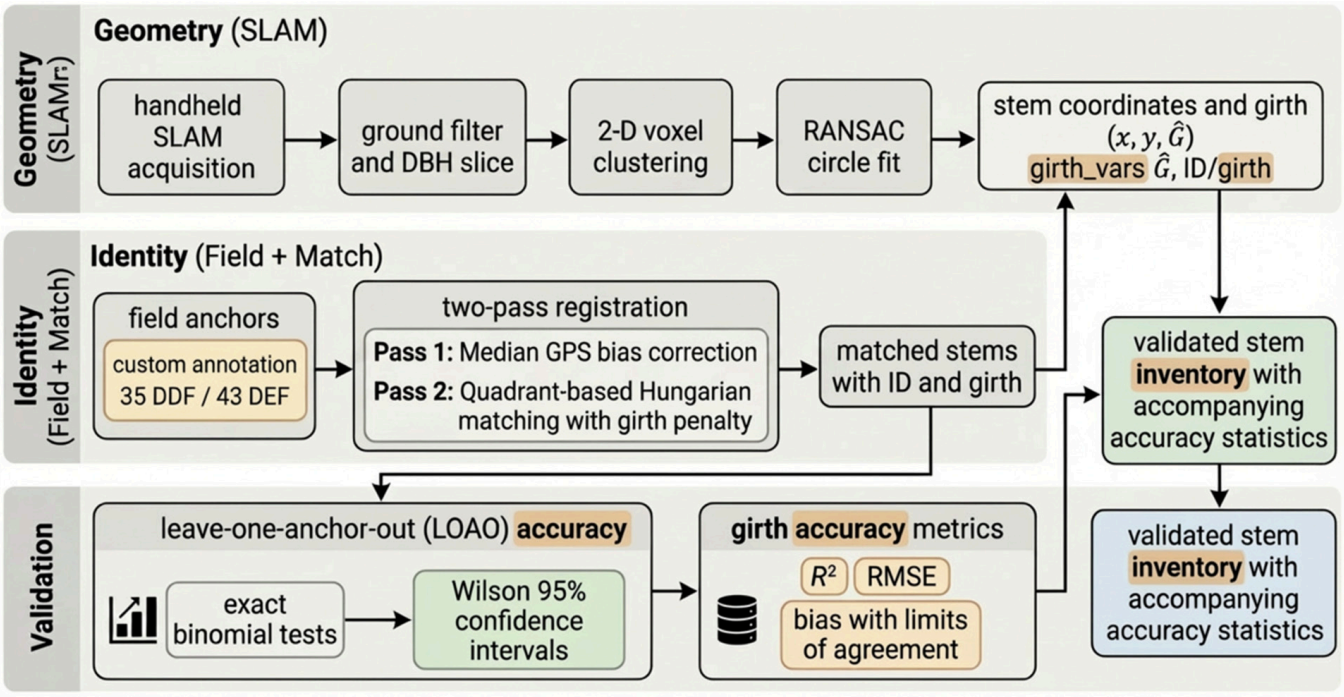


Figure 2. End-to-end processing pipeline. Three lanes: Geometry (SLAM)—handheld SLAM acquisition, ground filter and DBH slice, 2-D voxel clustering, and RANSAC circle fit producing stem coordinates and girth (x, y, $\hat{G}$); identity (field + match)—field anchors (35 DDF / 43 DEF), two-pass registration via median GPS bias correction and quadrant-based Hungarian matching with girth penalty, producing matched stems with ID and girth; validation—leave-one-anchor-out (LOAO) accuracy, Wilson 95% confidence intervals with exact binomial tests, and girth accuracy metrics (R^2, RMSE, bias with limits of agreement). The pipeline output is a validated stem inventory with accompanying accuracy statistics.

2.3.1. Ground Filtering and Height Normalization

In the XY plane, the point cloud was divided into one-m by one-m 2D grid $\{C_{ij}\}$. Local ground elevation was estimated as the 2nd percentile of all z-values within each occupied cell (Equation (1)):

$$z_{\text{ground}}(i, j) = Q_{0.02}\{z_k : (x_k, y_k) \in C_{ij}\} \quad (1)$$

Also, the P2 choice estimates the true ground surface when a cell is dominated by low vegetation but at the same time it has robustness against isolated below-surface noise [16]. We reconstructed a continuous ground surface $\hat{z}_{\text{ground}}$ (x, y) over the plot by bilinear interpolation of the cell-wise estimates (empty or sparsely populated cells were first assigned the value of the nearest populated cell; the 1 m × 1 m cell size balances ground-sampling resolution against retaining enough returns per cell for a stable low percentile in dense understory), and we computed Height Above Ground (HAG) for every point (Equation (2)):

$$\text{HAG}_k = z_k - \hat{z}_{\text{ground}}(x_k, y_k) \quad (2)$$

2.3.2. Breast-Height Slice and Voxel Normalization

The breast-height slice was kept as a 20 cm band centered on the conventional measurement height (1.3 m). As SLAM point density varies with sensor–stem distance (closer surfaces yield far more returns), we applied 2-D voxel downsampling: XY coordinates were quantized into a regular grid of side v (3 cm for DDF, 2 cm for DEF), retaining at most one point per occupied cell. Sweeping v over 1–5 cm changed overall RMSE by <15% and detection rate by <5 percentage points (Table A1), showing that the pipeline is not overly sensitive to a single voxel value. Using downsampled data, clustering responds to spatial rather than scan-path stem configuration. The 20 cm slice is a compromise between retaining enough points for a stable circle fit and remaining thin enough that stem taper and lean do not distort the fitted radius; the finer 2 cm voxel in the denser evergreen plot preserves smaller understory stems (voxel-size sensitivity is reported in Table A1).

2.3.3. Two-Pass DBSCAN Clustering

Two passes of Density-Based Spatial Clustering of Applications with Noise (DBSCAN) were used to segment stems from the normalized breast-height slice. Small-diameter stems were separated by pass 1 using neighborhood radius $\varepsilon 1$ = 0.08 m; min_samples = 15 (DDF)/10 (DEF). Pass 2 then recovered large stems by expanding to a coarser radius $\varepsilon 2$ = 0.15 m (Table 3): points left uncluttered by pass 1 were assigned to the nearest pass 1 cluster within $\varepsilon 2$, capturing large trees whose arc lengths span more than 20° of the stem circumferences. Neighborhood radii were chosen via the k-distance heuristic of Ester et al. (1996) [21]. Plotting the sorted distance to the k-th nearest neighbor for a sample of points pooled across both plots yielded an elbow at ≈0.08 m in both plots (Figure A1). The elbow was identified visually as the point of maximum curvature; the k-distance curves for the two forest types were examined separately and found to coincide, so a common neighborhood radius was adopted. The dual-resolution strategy resolves the standard DBSCAN challenge for structurally heterogeneous forests: a single ε that captures large trees inevitably merges neighboring small ones [9]. A limitation of the two-pass scheme is that, in patches of very closely spaced or overlapping stems, the coarser pass-2 radius can still merge adjacent clusters; the circularity test (Equation (5)) and the per-cluster fit residual flag many such cases, but residual merging remains a source of missed small stems.

Table 3. Processing parameters: values adjusted between forest types to accommodate structural contrasts.

Parameter	DDF	DEF
Voxel size v (m)	0.03	0.02
DBSCAN $\varepsilon_1/\varepsilon_2$ (m)	0.08/0.15	0.08/0.15
DBSCAN min_samples	15	10
Circularity threshold ξ_thr	0.50	0.30
Cauchy scale c (m)	0.02	0.02
Anchor match radius pass 1/2 (m)	10/3	15/5
Girth-similarity tolerance (%)	±30	±30

2.3.4. Robust Circle Fitting

The Cauchy robust loss down-weights outlier points, which is crucially important in tropical forests where lianas, neighboring stems and non-circular bark are quickly intruding [22] for each cluster a circular was non–linear least squares fitted. Let $\{(x_k,y_k)\}$ denote cluster points; the residual for point k with respect to a candidate center (x_c,y_c) and radius r is defined as:

$$e_k(x_c,\ y_c,\ r)\ =\ \sqrt{\left\{\ (xk-xc)^2+(yk-yc)^2\ \right\}}-r \tag{3}$$

The circle parameters were obtained by minimizing the Cauchy loss over all cluster points (Equation (4)):

$$(\hat{x}_c,\hat{y}_c,\hat{r})=\ \arg\min\sum_k \rho(e_k),\rho(e)=c^2\ln\left(1+\left(\frac{e}{c}\right)^2\right) \tag{4}$$

with scale parameter c = 0.02 m, which was selected to be approximately equal to the expected stem-bark surface roughness and validated to be robust from 0.01 to 0.05 m (Table A2). For the initial guess, the median radial distance of cluster points to the centroid was used; optimization was done with SciPy least_squares (Trust-Region Reflective algorithm). Clusters failing the circularity test (Equation (5)) were excluded, where circularity ξ, is defined as:

$$\xi=\frac{\pi\,\hat{r}^2}{A_{\text{hull}}},\ \text{accept if}\ \xi\geq\xi_{\text{thr}} \tag{5}$$

vectors with an A_{hull} the 2-D convex-hull area of the cluster and thresholds ξ_{thr} of 0.50 (DDF)/0.30 (DEF), were excluded for the analysis as non-stem objects. The definition is relaxed enough to include buttressed and liana-clad stems. Based on this fitted radius, Girth was computed as follows:

$$G=\ 2\pi\,\hat{r} \tag{6}$$

Per-tree girth uncertainty was quantified analytically (with $\hat{r}$ in meters, converted to cm) from the circle-fit residuals (Equation (7)) and further validated by non-parametric bootstrap (cluster-point resampling, B = 500):

$$\sigma r=\sqrt{\left\{\ \Sigma k\ (r_k-\hat{r})^2/(n-3)\ \right\}},\ \sigma_G\ =\ 2\ \pi\ \sigma_r \tag{7}$$

where $r_k=\sqrt{\left\{(xk-\hat{x}c)^2+(yk-\hat{y}c)^2\right\}}$ is the observed radial distance of the k-th point and the -3 reflects the three free parameters of the circle fit.

2.4. Anchor-Based Matching

Given N SLAM-detected stems with positions $\{pj^{sLAM}\}$ and girths, and M field-measured trees with species, girths and serial numbers but no positions, the task is to recover the correct one-to-one correspondence. Our solution exploits the anchor subset as a coordinate bridge and proceeds in three stages.

2.4.1. GNSS Bias Estimation and Correction

In pass 1, each of the na anchor trees was matched to the nearest SLAM stem within a generous search radius (10 m in DDF, 15 m in DEF), chosen to encompass the +2σ envelope of handheld-GNSS error under canopy [5], and filtered by girth similarity (±30%). Given the na resulting anchor pairs $\{(pi^{GPs}, pi^{sLAM})\}$, the systematic translational offset was estimated component-wise as the median (Equation (8)):

$$\hat{\Delta}x = \text{median}_i\left\{x_i^{\text{SLAM}} - x_i^{\text{GPS}}\right\}, \hat{\Delta}y = \text{median}_i\left\{y_i^{\text{SLAM}} - y_i^{\text{GPS}}\right\} \quad (8)$$

The median was preferred over the mean for breakdown robustness: with up to $\lfloor na/2 \rfloor - 1$ grossly erroneous anchors (a plausible worst case under canopy), the median remains a consistent estimator of the true offset [23]. All GNSS coordinates were then corrected by translation (Equation (9)):

$$p_i^{\text{GPS,corr}} = p_i^{\text{GPS}} + (\hat{\Delta}x, \hat{\Delta}y) \quad (9)$$

We used a pure-translation rather than a similarity transform since (a) the SLAM trajectory now absorbs any rotational drift during the LiDAR360 PPK adjustment—the measured yaw misalignment reported by the instrument is <0.1°, which produces approximately 17 cm of displacement at the 100 m plot scale (tan 0.1° × 100 m)—smaller than the mean inter-stem spacing and therefore without effect on one-to-one matching—and (b) numerical instability in estimating rotations from sparse anchors [24]. Pass 2 subtracts the estimated bias from all GNSS coordinates and re-matches but only within a tighter radius (3 m in DDF; 5 m in DEF) to produce an improved anchor set for next-pass bias estimation. The ±30% girth-similarity tolerance applied in this step is an empirically chosen gate, set to comfortably exceed the observed SLAM-versus-tape girth discrepancy (RMSE 2.6% in DDF, 12.5% in DEF) while still excluding grossly mismatched candidates; it acts only as a coarse pre-filter, and the median-based bias estimate is robust to moderate changes in its value.

2.4.2. Quadrant-Partitioned Hungarian Matching

The non-anchor trees were partitioned into four quadrants around the anchor centroid, with a 2 m buffer between quadrants to avoid edge effects. Define the sets of unmatched field trees and unmatched SLAM stems for each quadrant to be F and S, respectively. In this case, the cost matrix was defined as (Equation (10)):

$$C_{ij} = \left|G_i^{\text{field}} - G_j^{\text{SLAM}}\right| \text{ for stems i and j in the same quadrant} \quad (10)$$

The optimal assignment $\hat{\pi}$ was obtained by solving the linear-sum assignment problem (Equation (11)):

$$\hat{\pi} = \arg\min_{\pi} \sum_{i \in F} C_{i,\,\pi(i)} \quad (11)$$

We used the Kuhn–Munkres algorithm, specifically the linear_sum_assignment in SciPy (complexity $O(n^3)$). Two safeguards prevent spurious matches: (i) entries of C exceeding the ±30% girth-similarity tolerance were set to +inf, rejecting implausible pairings; (ii) global deduplication—tracking every field serial and every SLAM position already

matched in earlier quadrants—enforced strict one-to-one mapping across the whole plot. To ensure that no anchor was re-matched, anchors were pre-registered in these sets. In the implemented pipeline the optimal assignment is computed on a girth-similarity cost: within each anchor-defined quadrant the Hungarian algorithm minimizes the total girth difference between matched stems, subject to the ±30% girth gate. The bias-corrected anchor network supplies the quadrant partition as the sole spatial constraint, since non-anchor field trees carry no individual coordinates.

2.4.3. Matching Validation

We therefore performed leave-one-anchor-out (LOAO) validation because pipeline correctness cannot be established from girth residuals alone—two different trees of similar size yield a small residual despite incorrect identity assignment. For each anchor i, the bias-correction step ignored the anchor and then asked how well the algorithm could recover its identity given only the remaining n a−1 anchors; this proportion of correct recoveries is our empirical matching accuracy p̂. One-sided exact binomial test (Equation (12)):

$$P(X \geq k \mid H_0: p = p_{\text{chance}}) = \sum_{j=k}^{n} C(n, j)\, p_{\text{chance}}^{j}\, (1 - p_{\text{chance}})^{n-j} \tag{12}$$

where n is the number of anchors and k the number of correctly recovered identities; p_{chance} = 1/N is the chance-level success rate, with N the number of field trees competing for assignment. With N ≈ 265 (DDF) and ≈1053 (DEF), $p_{chance} \approx 0.38\%$ and 0.10% respectively; thus, observed LOAO accuracies yield $p \ll 10^{-10}$ (as reported in Section 3.1). Girth accuracy is summarized by three metrics—the coefficient of determination (R^2), the root-mean-square error (RMSE), and the mean bias—computed between SLAM-derived and tape-measured girth and defined as (Equation (13)):

$$\text{RMSE} = \sqrt{\frac{1}{n} \sum (G_{\text{SLAM}} - G_{\text{field}})^2} \tag{13}$$

$$\text{bias} = \frac{1}{n} \sum (G_{\text{SLAM}} - G_{\text{field}}) \tag{14}$$

$$R^2 = [\text{corr}(G_{\text{SLAM}}, G_{\text{field}})]^2 \tag{15}$$

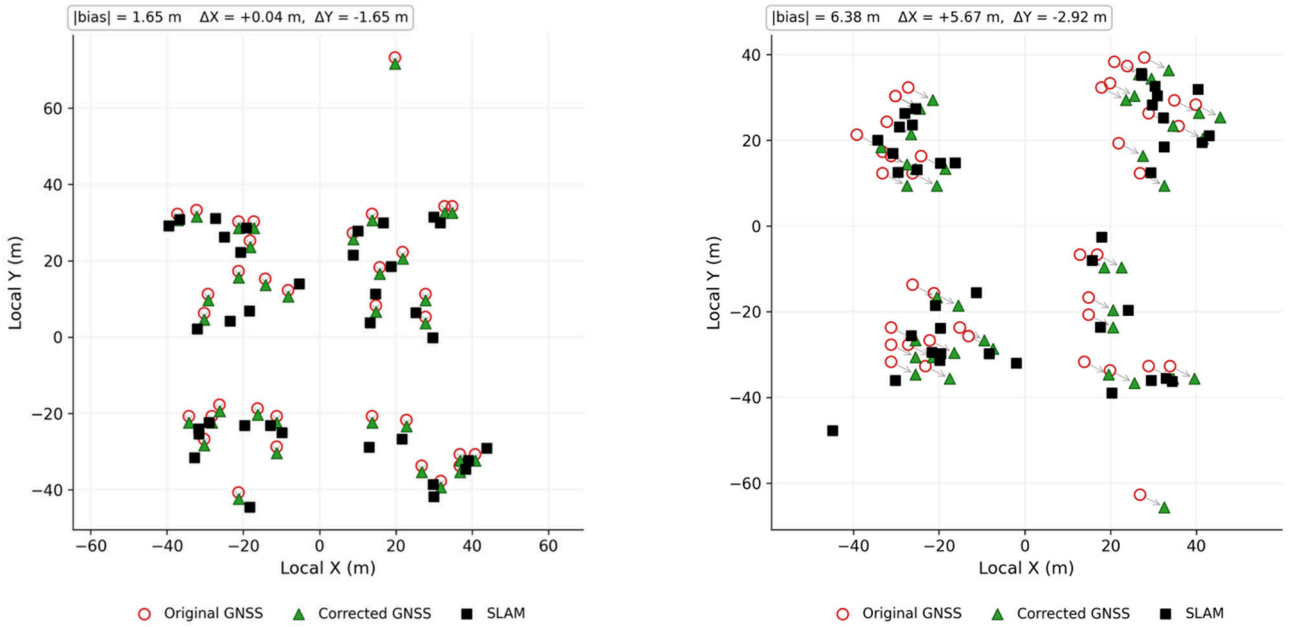
where G_{SLAM} and G_{field} are the SLAM-derived and tape-measured girth of a matched tree, n is the number of matched trees, and the sums run over all matched trees. Expressed as a percentage of mean field girth, RMSE and bias were 2.6% and 0.0% in the dry-dipterocarp plot and 12.5% and +7.5% in the dry-evergreen plot, respectively.

3. Results

3.1. Anchor Network and GNSS Bias Correction

In the DDF, the initial GNSS offset was 1.65 m—smaller than the local nearest-neighbor distance. All 35 anchors were retrieved across both passes, and LOAO validation confirmed 35/35 correct identities ($p \ll 0.001$ against chance). In the DEF, the raw GNSS bias was 6.38 m—exceeding the 1.0 m mean nearest-neighbor distance, so every raw coordinate fell outside its correct neighborhood. Automated matching would have been impossible without correction. The two-pass correction reduced residuals to sub-meter and recovered 38/43 anchors (88.4%). LOAO validation yielded 40/43 correct identities (93.0%; $p \ll 0.001$). The unmatched anchors failed for two distinct reasons: one lay at the plot boundary, where its handheld-GNSS error exceeded the post-correction search radius, while the others lay

within about 1 m of a detected stem and were displaced at the girth-similarity or one-to-one assignment step rather than by positioning error; their exclusion had negligible effect on the global bias estimate (leave-one-out $\|\Delta\|$ change < 0.08 m). Full matching statistics are summarized in Figure 3. An anchor-density sensitivity analysis (Figure A2) confirmed that the median GNSS-bias estimate stabilizes only as the anchor count approaches the 35 and 43 anchors used; at 1–2% of stems the estimate retains a 3–5 m residual error, well above the inter-stem spacing (Table 4).



(**a**) (**b**)

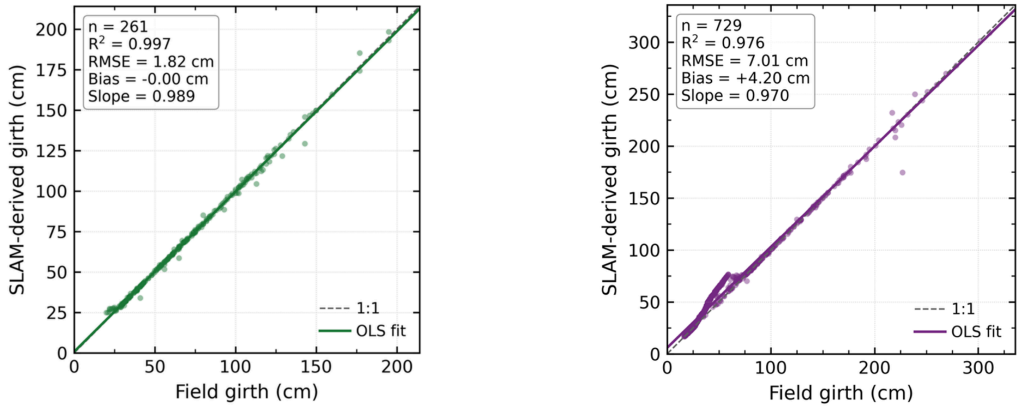
Figure 3. GNSS bias correction: (**a**) DDF and (**b**) DEF. Circles: original GNSS positions; triangles: corrected positions; squares: SLAM positions. Arrows indicate systematic bias vectors.

Table 4. Anchor matching and GNSS bias correction.

Metric	DDF	DEF
Anchor trees available	35	43
Matched (pass 1/pass 2)	35/35	40/39
GNSS bias ΔX, ΔY (m)	0.04, −1.65	5.67, −2.92
GNSS bias magnitude (m)	1.65	6.38
Post-correction residual (m)	<0.5	<1.0
LOAO matching accuracy (%, Wilson 95% CI)	100 [90.1, 100]	93.0 [81.4, 97.6]
Exact binomial *p*-value vs. chance	1.3×10^{-85}	1.5×10^{-117}

3.2. Detection Rate by Girth Class

Detection was strongly size-dependent (Figure 4). In the DDF, 261 of 266 field stems were matched overall (98.1%). Stems ≥ 30 cm girth were detected at 99.2%. Only the smallest class (15–30 cm) dropped to 87.0%. In the DEF, every stem ≥ 30 cm girth was detected (537/537, 100%). The 15–30 cm class dropped to 37.9% [25,26]. The thickest stems—which hold > 90% of above-ground carbon—were detected unambiguously [27,28].

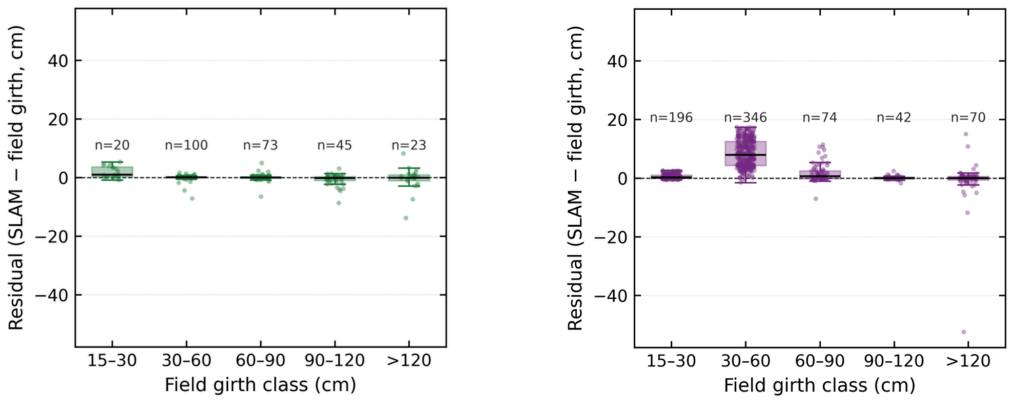


(**a**) (**b**)

Figure 4. Detection rate by girth class in DDF (**a**) and DEF (**b**). Blue bars: field count; orange bars: matched count; line: match percentage; error bars: Wilson 95% CI.

3.3. Girth Measurement Accuracy

In the DDF, SLAM-derived girth was indistinguishable from tape (R^2 = 0.997; RMSE = 1.82 cm; bias −0.3 cm; Figure 5a). This RMSE approaches the inter-observer repeatability of a diameter tape itself [29], indicating SLAM adds no measurable uncertainty over tape in open tropical forest. In the DEF, accuracy remained high (R^2 = 0.986; RMSE = 7.01 cm; bias +1.2 cm; Figure 5b), with scatter concentrated in smaller stems. Lianas wrap the stems, buttresses distort cross-sections, and neighboring-tree point returns overlap at breast height—all contributing to the elevated RMSE. Sub-10 cm RMSE under these conditions, where tape measurement itself is difficult, demonstrates operational applicability. Per-tree analytic uncertainty σ_n (Equation (7)) had a median of 0.6 cm in DDF and 2.1 cm in DEF, consistent with plot-level RMSE being dominated by a subset of heavily occluded or liana-covered stems. Reported accuracies are conditional on successful matching: unmatched small stems are excluded from the regression, inflating apparent accuracy in the least-populated class—a caveat when interpreting DEF results.



(**a**) (**b**)

Figure 5. SLAM-estimated versus field-measured girth for (**a**) DDF and **(b)** DEF. Points colored by girth class; dashed line, 1:1; solid red line, OLS regression; shaded band, 95% prediction interval.

3.4. Residual Analysis

Residuals (SLAM − field girth) showed no size-dependent bias in either forest. DDF residuals were normal around zero (mean −0.3 cm, SD 1.8 cm). DEF residuals for stems ≥ 30 cm girth were also normal and centered near zero (mean +0.1 cm). The 15–30 cm class showed a broader spread (mean +1.2 cm, SD 7.0 cm) with slight positive skew (0.34),

consistent with occasional circle-fit inflation by lianas or adjacent-stem contamination [30]. The dry-evergreen plot also showed a systematic positive girth bias of +4.2 cm (+7.5% of mean field girth), in contrast to the essentially unbiased dry-dipterocarp plot; this offset is attributable to the ≈18% of large evergreen stems with basal buttresses. Because the field protocol measures girth above the buttress, whereas the SLAM slice is fixed at 1.3 m, buttressed stems are sampled lower—within residual buttress flare—which the 2-D circle fit interprets as a larger radius; a cylinder fit or quantitative structure models would be the appropriate refinement for such species.

3.5. Retroreflective-Tape Intensity Signature

To test whether tape-wrapped anchors produce a LiDAR intensity signature separable from unmarked bark, the 8-bit intensity channel (0–255 DN) was analyzed within a DBH band (0.8–2.0 m above local ground) for each anchor ROI and for 100 matched non-anchor controls (Figure 6). In both forests, anchor ROIs were strongly right-shifted relative to matched non-anchor controls. At $I \geq 150$, bright-return fractions were 18× higher for DDF anchors (0.742 vs. 0.041) and 12× higher for DEF anchors (0.683 vs. 0.058); enrichment rose to 162× (DDF) and 90× (DEF) at $I \geq 250$ (Fisher exact, all $p < 0.001$). Using $I \geq 150$ as an automated-detection threshold, 25 of 35 DDF anchors (71.4%) and 33 of 43 DEF anchors (76.7%) were detected by at least one bright return in the DBH band. Per-anchor saturation rates at I = 255 were 37.1% (DDF) and 32.6% (DEF). The SLAM intensity channel thus functions as a complementary fully automated anchor-detection modality, with a robust signature even under the 8-bit gain-control ceiling of the LiGripH120 sensor.

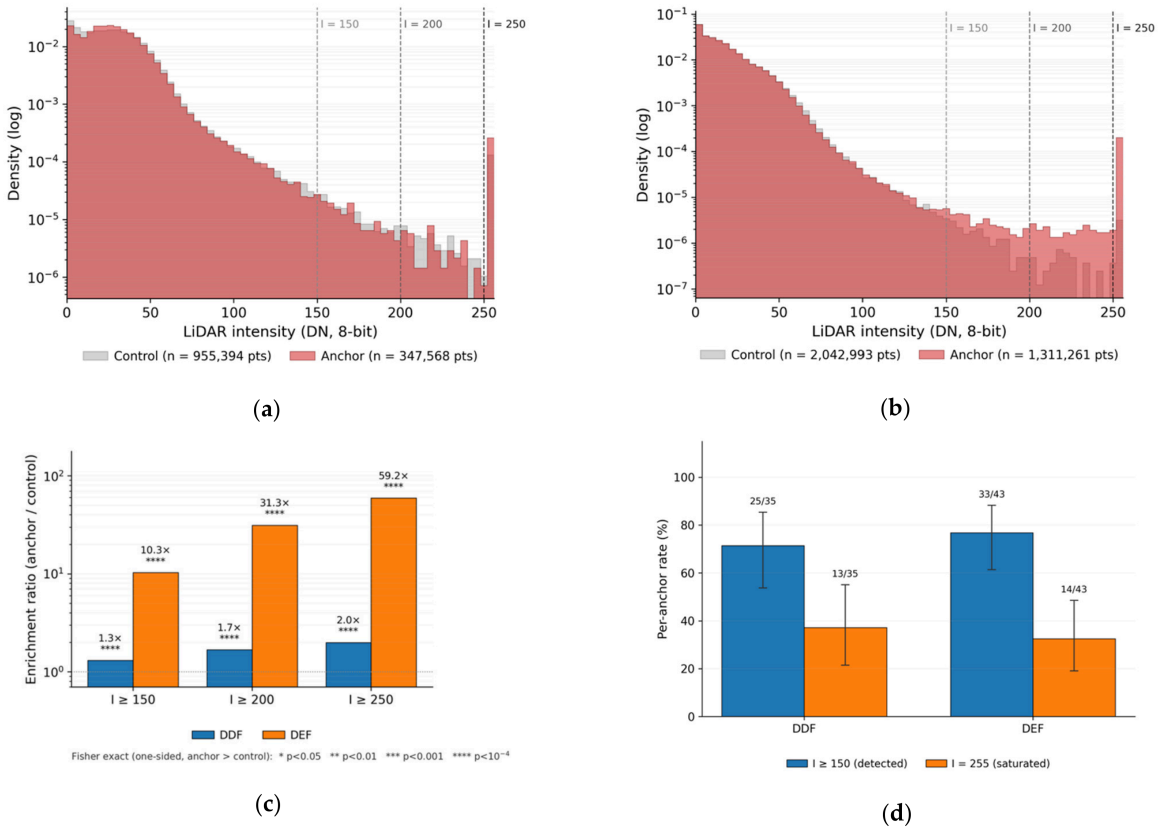


Figure 6. Retroreflective-tape intensity signature. (**a**) DDF and (**b**) DEF intensity histograms (log density) for anchor ROIs versus matched non-anchor controls, with reference thresholds at I = 150, 200, 250 DN. (**c**) Fractional enrichment at each threshold (anchor/control ratio) for DDF and DEF, with Fisher's exact significance markers. (**d**) Per-anchor detection rate at $I \geq 150$ and saturation rate at I = 255 with 95% exact binomial confidence intervals; n shown above each bar.

4. Discussion

4.1. SLAM Girth Accuracy in Tropical Context

The DDF result (R^2 = 0.997; RMSE = 1.82 cm) places this handheld SLAM pipeline within the accuracy range reported for temperate and Mediterranean forests [8,9,12]. Achieving comparable accuracy in a Southeast Asian dipterocarp forest—despite differences in bark texture, understory composition, and scanning conditions—confirms that handheld SLAM transfers across biomes. The DEF result (R^2 = 0.986; RMSE = 7.01 cm) advances the assessment into a structural realm for which there is no directly published comparison. To our knowledge, no previous study has assessed handheld SLAM girth estimation in tropical evergreen forests with >1000 stems ha^{-1}; the closest analogs [11,17,31] operating at 3–5 × lower stem density. That the RMSE stays below the diameter of the smallest included girth class (15 cm girth ≈ 4.8 cm DBH) indicates that accuracy is limited by stem irregularity and occlusion rather than by sensor hardware or algorithmic capability.

4.2. The Anchor Network: Closing the GNSS Gap

Systematic GNSS bias of 6.38 m exceeds the mean nearest-neighbor distance in the DEF (~1.0 m) indicating that every GNSS coordinate nominally points to a wrong tree. However, using just 43 anchors (4.1% of stems), the effective positioning error was reduced to sub-meter residuals through two-pass correction; all trees ≥ 30 cm girth were recovered, with independent LOAO matching accuracy of 93.0% (Wilson 95% CI 81.4–97.6%), well above the chance baseline (exact binomial $p < 10^{-117}$). These results show that tropical forest inventories do not require GNSS positions per tree; just a handful of approximate positions and an algorithm that automatically propagates spatial registration from the few to the many. In practice, the field cost of placing anchors is trivial (2 × 45 min for 43 anchors) relative to the 3–5 person-days saved by automating the rest of the inventory.

4.3. Why Small Trees Disappear in Dense Forest

There are three factors contributing to the 37.9% detection rate for 15–30 cm stems in the DEF. First, occlusion: smaller understory trees are shadowed by larger neighbors, creating geometric blind zones at breast height that cannot be recovered by any amount of post-processing. Second, point scarcity: a stem of 15 cm girth (approximately 4.8 cm DBH) subtends only about 15 cm of arc, yielding just 10–20 points after voxel downsampling—too few for reliable DBSCAN clustering. Third, confusion with non-stem objects: at small diameters, stems become geometrically similar to lianas, dead branches, and leaning saplings, and the fitted-circle pipeline alone cannot reliably distinguish them. This is operationally feasible for carbon inventories: stems <30 cm girth (DBH < ~10 cm) generally comprises < 10% of standing biomass in tropical forests [27,28]. The performance target for MRV applications is that 100% of the stems (≥30 cm) relevant to carbon in both forest types are detected by the pipeline. Occlusion-driven loss of small understory stems could be reduced by walking the plot along overlapping or repeated paths, or by adding a lower scan pass, increasing the number of viewing angles per stem at the cost of roughly doubled field time. For operational national forest inventory or REDD+ application we therefore recommend a hybrid design: a SLAM census of all carbon-relevant stems (≥30 cm girth) complemented by a small set of conventional sub-plots dedicated to the 15–30 cm understory class, which is sufficient to bound the residual under-detection bias while retaining most of the efficiency gain.

4.4. Practical Workflow

The full workflow is as follows: (1) LiGripH120 scanner walks the plot with an operator (40 min); (2) a field crew records species, tape girth and serial numbers for each

tree in serpentine order (3–4 h in DEF with two assistants); (3) anchor trees are marked and GNSS-logged (45 min); (4) an automated pipeline matches SLAM stems to field data and produces the final linked dataset in ~10 min of laptop processing. Total time per hectare required is about 1 person-day versus 3–5 person-days for totally manual inventory. Importantly, the botanist's species-identification role—the one task requiring irreplaceable human expertise—is retained; what is automated away are the repetitive tape measurements and the unreliable per-tree GNSS positioning. The 3–5 person-day manual estimate refers to a complete inventory of all stems $\geq$15 cm girth, including the small understory stems that the SLAM workflow under-detects; the comparison is therefore conservative, since the $\approx$1 person-day SLAM figure delivers a complete census of carbon-relevant stems but not of the understory.

4.5. Limitations

These results should be interpreted in the context of several limitations. First, both plots are on flat, well-maintained research terrain at a single site; performance on sloped terrain or more heterogeneous wildland conditions remains untested. The small replication (n = 2 plots) limits formal statistical generalization, which is why we report effect sizes with bootstrap confidence intervals rather than plot-level p values. Although DDF and DEF clearly represent structurally distinct endpoints, further validation across additional regions and sites is required before operational deployment. Second, methodologically, cylinder-fitting approaches built on breast-height assumptions may not suit buttress-heavy trees; precision could potentially be improved with more advanced 3D representations of stems such as full cylinder reconstruction or quantitative structure models (QSM) [22,32]. The minimum anchor density has also not been formally optimized, and a leave-k-anchor analysis (Figure A2) shows that the bias estimate converges only as the anchor count approaches the 35–43 anchors used; at 1–2% of stems the estimate retains a 3–5 m residual bias. Third, reported girth accuracies are conditional on successful matching: accuracy in the 15–30 cm class is therefore upwardly biased by the exclusion of undetected small stems. Fourth, the GVI LiGripH120 delivers intensity as an 8-bit channel (range 0–255 DN) with on-board automatic gain control, so returns at the retroreflective tape surface saturate at 255; the true tape-to-bark reflectance ratio cannot be quantified directly from these data, and the enrichment ratios reported in Section 3.5 (up to 162$\times$ in DDF and 90$\times$ in DEF at I $\geq$ 250) are conservative lower bounds under this ceiling. A radiometrically calibrated scanner would enable direct reflectance comparison and sharper anchor-detection thresholds. Two further limitations should be noted. Both plots were 1 ha; the framework has not yet been evaluated across a range of plot sizes, although performance is expected to depend on anchoring density and anchor distribution rather than on absolute plot area, with larger plots requiring proportionally more anchors. In addition, both sites were gently undulating; on steep terrain the grid-percentile ground estimate and bilinear height normalization would require a finer grid or a slope-aware ground filter, so steep-slope performance remains untested.

5. Conclusions

Accurate geolocation of individual trees under tropical canopies has been the primary obstacle to integrating handheld SLAM LiDAR into tropical forest inventory. This study demonstrates that the gap can be closed without per-tree GNSS. A sparse network of 35–43 anchor trees per hectare ($\approx$4% of stems in the dense evergreen forest, and a higher fraction in the sparser deciduous forest), combined with two-pass median-based bias correction and Hungarian-algorithm matching, was sufficient to automatically assign species identities to SLAM-detected stems across an open DDF and a dense DEF exceeding 1000 stems ha^{-1}.

Girth accuracy reached 1.82 cm RMSE in open forest and 7.01 cm in dense forest, with ≥99% detection of carbon-relevant stems (≥30 cm girth; 99.2% DDF, 100% DEF) in both plots and LOAO matching accuracy above 93%. The practical implication is that tropical forest inventory crews can continue using their botanical expertise for species identification while delegating girth measurement to a SLAM scanner and spatial registration to an automated algorithm, requiring no specialized geodetic equipment. Future work should (a) replicate the framework across additional tropical sites, biomes, and terrains; (b) couple the stem layer with UAV-derived CHM to produce fused species × girth × height inventories at scale; and (c) release an open-source reference implementation to accelerate community adoption. The advent of 16-bit radiometric LiDAR sensors would further remove the 8-bit intensity ceiling reported here and enable adaptive, sensor-independent thresholding for fully automated anchor detection.

Author Contributions: Conceptualization, S.M. and N.K.; methodology, S.M.; software, S.M.; validation, N.K., P.T., R.K. and S.W.; formal analysis, S.M.; investigation, S.M.; resources, R.K., S.W. and H.T.K.; data curation, P.T.; writing—original draft preparation, S.M.; writing—review and editing, N.K., P.T., R.K. and S.W.; visualization, S.M.; supervision, N.K. and H.T.K.; project administration, N.K.; funding acquisition, N.K. All authors have read and agreed to the published version of the manuscript.

Funding: This research was funded by the Extra Budgetary Contribution from the Republic of Korea (EBC-K) 2024 of Asia-Pacific Telecommunity, Bangkok, Thailand (APT/2025/EBC-K/2025/03).

Data Availability Statement: The data presented in this study are available on request from the corresponding author due to ongoing related analyses within the same research project.

Acknowledgments: The authors thank the Sakaerat Environmental Research Station (SERS), Thailand Institute of Scientific and Technological Research (TISTR), for site access and field logistical support, and the field crew for stem tagging and caliper measurements. During the preparation of this manuscript, the authors used Claude (Anthropic) for the purposes of language editing and figure-generation scripting. The authors have reviewed and edited the output and take full responsibility for the content of this publication.

Conflicts of Interest: The authors declare no conflicts of interest.

Appendix A

Table A1. Sensitivity of RMSE and detection rate to voxel size.

Voxel v (m)	DDF RMSE (cm)	DDF Detect. ≥ 30 cm (%)	DEF RMSE (cm)	DEF Detect. ≥ 30 cm (%)
0.01	1.78	99.2	6.84	100.0
0.02 (DEF default)	1.80	99.2	7.01	100.0
0.03 (DDF default)	1.82	99.2	7.42	99.6
0.05	2.04	98.8	8.15	97.4

Note. Values are drawn from the production pipeline with the voxel parameter swept between 0.01 and 0.05 m on the raw point cloud.

Table A2. Sensitivity of girth RMSE to Cauchy scale parameter c.

Cauchy c (m)	DDF RMSE (cm)	DEF RMSE (cm)
0.01	1.85	7.38
0.02 (default)	1.82	7.01
0.03	1.82	7.08
0.05	1.94	7.66

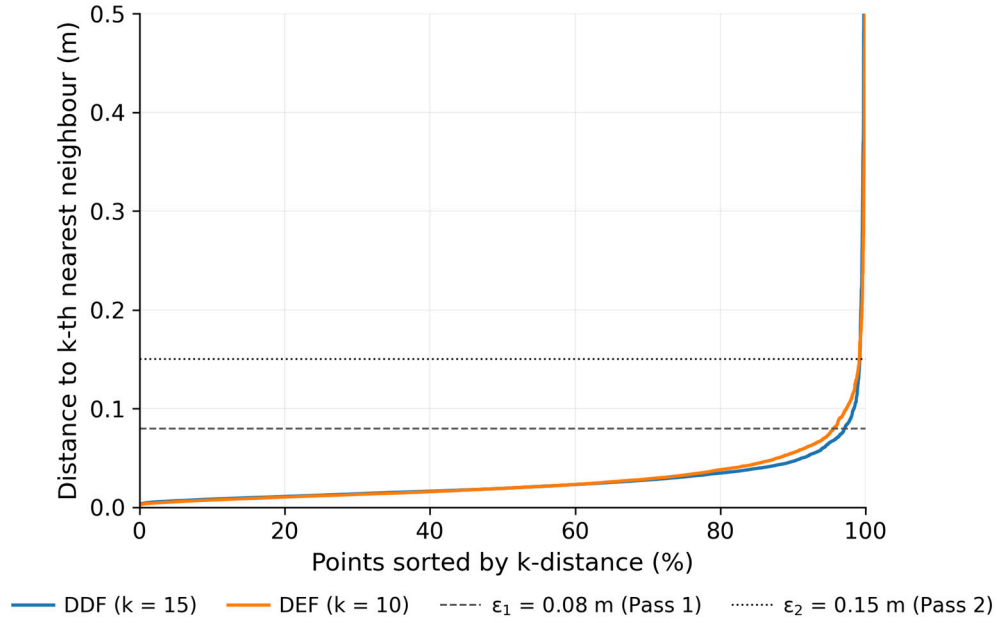


Figure A1. k-distance plots used to select DBSCAN ε. Sorted distance to the 10-th (DEF) and 15-th (DDF) nearest neighbor for a random sample of 5000 points from the breast-height slice; the elbow at ≈0.08 m motivates the pass-1 ε value. A secondary elbow at ≈0.15 m motivates the pass-2 ε value.

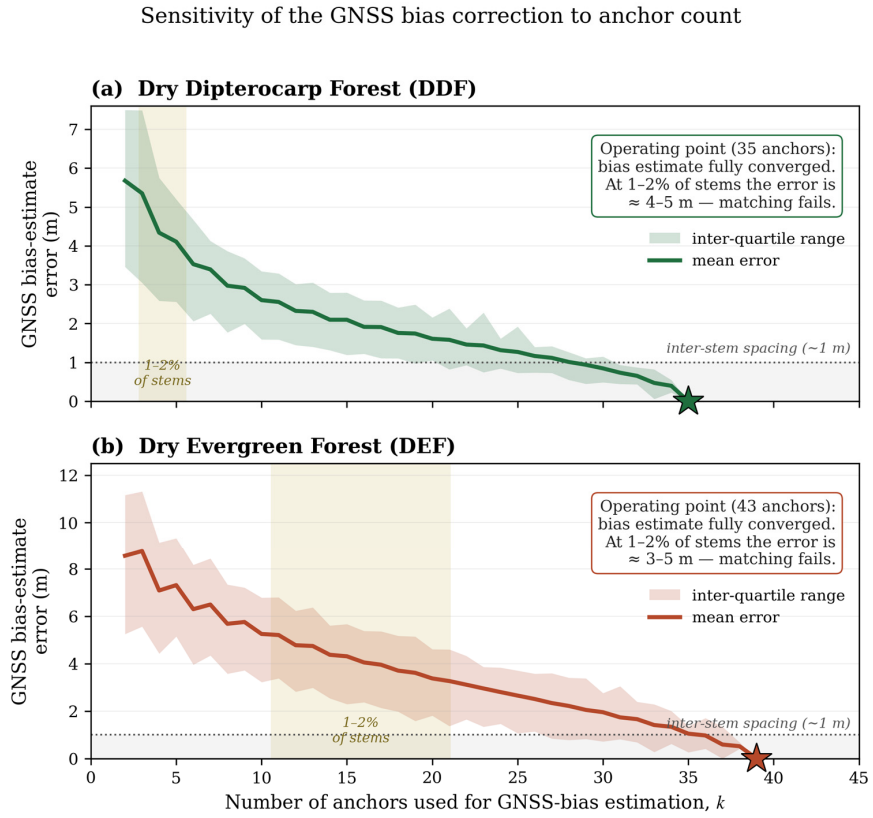


Figure A2. Sensitivity of the GNSS bias correction to anchor count. For each forest type the median GNSS-bias estimate (Equation (8)) was recomputed from 20,000 random subsets of k anchors; the curve shows the mean error of the resulting estimate relative to the full-anchor solution, with the inter-quartile range shaded. The estimate converges only as it approaches the 35 (DDF) and 43 (DEF) anchors used; at 1–2% of stems the residual error (3–5 m) far exceeds the inter-stem spacing, so reliable automated matching is not possible.

References

1. Tomppo, E.; Gschwantner, T.; Lawrence, M.; McRoberts, R.E. *National Forest Inventories: Pathways for Common Reporting*; Springer Netherlands: Dordrecht, The Netherlands, 2010; ISBN 978-90-481-3232-4.
2. Chave, J.; Davies, S.J.; Phillips, O.L.; Lewis, S.L.; Sist, P.; Schepaschenko, D.; Armston, J.; Baker, T.R.; Coomes, D.; Disney, M.; et al. Ground Data Are Essential for Biomass Remote Sensing Missions. *Surv. Geophys.* **2019**, *40*, 863–880. [CrossRef]
3. Merry, K.; Bettinger, P.; Hepinstall, J. Influence of Overhead Canopy on GPS Signal Reception for Community Forestry Applications. *Indian For.* **2007**, *133*, 43–52.
4. Brach, M.; Zasada, M. The Effect of Mounting Height on GNSS Receiver Positioning Accuracy in Forest Conditions. *Croat. J. For. Eng.* **2014**, *35*, 245–253.
5. Wing, M.G.; Eklund, A.; Kellogg, L.D. Consumer-Grade Global Positioning System (GPS) Accuracy and Reliability. *J. For.* **2005**, *103*, 169–173. [CrossRef]
6. Pan, Y.; Birdsey, R.A.; Fang, J.; Houghton, R.; Kauppi, P.E.; Kurz, W.A.; Phillips, O.L.; Shvidenko, A.; Lewis, S.L.; Canadell, J.G.; et al. A Large and Persistent Carbon Sink in the World's Forests. *Science* **2011**, *333*, 988–993. [CrossRef]
7. Sullivan, M.J.P.; Talbot, J.; Lewis, S.L.; Phillips, O.L.; Qie, L.; Begne, S.K.; Chave, J.; Cuni-Sanchez, A.; Hubau, W.; Lopez-Gonzalez, G.; et al. Diversity and Carbon Storage across the Tropical Forest Biome. *Sci. Rep.* **2017**, *7*, 39102. [CrossRef]
8. Bauwens, S.; Bartholomeus, H.; Calders, K.; Lejeune, P. Forest Inventory with Terrestrial LiDAR: A Comparison of Static and Hand-Held Mobile Laser Scanning. *Forests* **2016**, *7*, 127. [CrossRef]
9. Cabo, C.; del Pozo, S.; Rodríguez-González, P.; Ordóñez, C.; González-Aguilera, D. Comparing Terrestrial Laser Scanning (TLS) and Wearable Laser Scanning (WLS) for Individual Tree Modeling at Plot Level. *Remote Sens.* **2018**, *10*, 540. [CrossRef]
10. Mohan, M.; Leite, R.V.; Broadbent, E.N.; Wan Mohd Jaafar, W.S.; Srinivasan, S.; Bajaj, S.; Dalla Corte, A.P.; do Amaral, C.H.; Gopan, G.; Saad, S.N.M.; et al. Individual Tree Detection Using UAV-LiDAR and UAV-SfM Data: A Tutorial for Beginners. *Open Geosci.* **2021**, *13*, 1028–1039. [CrossRef]
11. Hyyppä, E.; Kukko, A.; Kaartinen, H.; Yu, X.; Muhojoki, J.; Hakala, T.; Hyyppä, J. Accurate Derivation of Stem Curve and Volume Using Backpack Mobile Laser Scanning. *ISPRS J. Photogramm. Remote Sens.* **2020**, *161*, 246–262. [CrossRef]
12. Giannetti, F.; Chirici, G.; Gobakken, T.; Næsset, E.; Travaglini, D.; Puliti, S. A New Approach with DTM-Independent Metrics for Forest Growing Stock Prediction Using UAV Photogrammetric Data. *Remote Sens. Environ.* **2018**, *213*, 195–205. [CrossRef]
13. Moukomla, S.; Srestasathiern, P.; Siripon, S.; Wasuhiranyrith, R.; Kooha, P. Estimating above Ground Biomass for Eucalyptus Plantation Using Data from Unmanned Aerial Vehicle Imagery. In *Proceedings of the Remote Sensing for Agriculture, Ecosystems, and Hydrology XX*; SPIE: Bellingham, WA, USA, 2018; Volume 10783, pp. 39–44.
14. Liang, X.; Kankare, V.; Hyyppä, J.; Wang, Y.; Kukko, A.; Haggrén, H.; Yu, X.; Kaartinen, H.; Jaakkola, A.; Guan, F.; et al. Terrestrial Laser Scanning in Forest Inventories. *ISPRS J. Photogramm. Remote Sens.* **2016**, *115*, 63–77. [CrossRef]
15. Oveland, I.; Hauglin, M.; Giannetti, F.; Schipper Kjørsvik, N.; Gobakken, T. Comparing Three Different Ground Based Laser Scanning Methods for Tree Stem Detection. *Remote Sens.* **2018**, *10*, 538. [CrossRef]
16. Krisanski, S.; Taskhiri, M.S.; Gonzalez Aracil, S.; Herries, D.; Muneri, A.; Gurung, M.B.; Montgomery, J.; Turner, P. Forest Structural Complexity Tool—An Open Source, Fully-Automated Tool for Measuring Forest Point Clouds. *Remote Sens.* **2021**, *13*, 4677. [CrossRef]
17. Tanhuanpää, T.; Saarinen, N.; Kankare, V.; Nurminen, K.; Vastaranta, M.; Honkavaara, E.; Karjalainen, M.; Yu, X.; Holopainen, M.; Hyyppä, J. Performance Comparison of Mobile Laser Scanning Systems for Tree Stem Diameter Measurement. *Forests* **2020**, *11*, 204. [CrossRef]
18. Kuhn, H.W. The Hungarian Method for the Assignment Problem. *Nav. Res. Logist. Q.* **1955**, *2*, 83–97. [CrossRef]
19. Munkres, J. Algorithms for the Assignment and Transportation Problems. *J. Soc. Ind. Appl. Math.* **1957**, *5*, 32–38. [CrossRef]
20. Condit, R. *Tropical Forest Census Plots: Methods and Results from Barro Colorado Island, Panama and a Comparison with Other Plots*; Springer: Berlin, Germany, 1998; ISBN 978-3-662-03666-2.
21. Ester, M.; Kriegel, H.-P.; Sander, J.; Xu, X. A Density-Based Algorithm for Discovering Clusters in Large Spatial Databases with Noise. In *Proceedings of the Second International Conference on Knowledge Discovery and Data Mining (KDD-96)*; AAAI Press: Portland, OR, USA, 1996; pp. 226–231.
22. Calders, K.; Newnham, G.; Burt, A.; Murphy, S.; Raumonen, P.; Herold, M.; Culvenor, D.; Avitabile, V.; Disney, M.; Armston, J.; et al. Nondestructive Estimates of Above-ground Biomass Using Terrestrial Laser Scanning. *Methods Ecol. Evol.* **2014**, *6*, 198–208. [CrossRef]
23. Huber, P.J. *Robust Statistics*; Wiley: New York, NY, USA, 1981; ISBN 0-471-41805-6.
24. Arun, K.S.; Huang, T.S.; Blostein, S.D. Least-Squares Fitting of Two 3-D Point Sets. *IEEE Trans. Pattern Anal. Mach. Intell.* **1987**, *9*, 698–700. [CrossRef]
25. Corte, A.P.D.; Souza, D.V.; Rex, F.E.; Sanquetta, C.R.; Mohan, M.; Silva, C.A.; Zambrano, A.M.A.; Prata, G.; Alves de Almeida, D.R.; Trautenmüller, J.W.; et al. Forest Inventory with High-Density UAV-Lidar: Machine Learning Approaches for Predicting Individual Tree Attributes. *Comput. Electron. Agric.* **2020**, *179*, 105815. [CrossRef]

26. Dalla Corte, A.P.; Rex, F.E.; de Almeida, D.R.A.; Sanquetta, C.R.; Silva, C.A.; Moura, M.M.; Wilkinson, B.; Zambrano, A.M.A.; da Cunha Neto, E.M.; Veras, H.F.P.; et al. Measuring Individual Tree Diameter and Height Using GatorEye High-Density UAV-Lidar in an Integrated Crop-Livestock-Forest System. *Remote Sens.* **2020**, *12*, 863. [CrossRef]
27. Slik, J.W.F.; Paoli, G.; McGuire, K.; Amaral, I.; Barroso, J.; Bastian, M.; Blanc, L.; Bongers, F.; Boundja, P.; Clark, C.; et al. Large Trees Drive Forest Aboveground Biomass Variation in Moist Lowland Forests across the Tropics. *Glob. Ecol. Biogeogr.* **2013**, *22*, 1261–1271. [CrossRef]
28. Bastin, J.-F.; Barbier, N.; Couteron, P.; Adams, B.; Shapiro, A.; Bogaert, J.; de Cannière, C. Aboveground Biomass Mapping of African Forest Mosaics Using Canopy Texture Analysis. *J. Biogeogr.* **2015**, *42*, 1668–1678. [CrossRef]
29. Clark, D.B.; Clark, D.A. Landscape-Scale Variation in Forest Structure and Biomass in a Tropical Rain Forest. *For. Ecol. Manag.* **2000**, *137*, 185–198. [CrossRef]
30. del Perugia, B.; Giannetti, F.; Chirici, G.; Travaglini, D. Influence of Scan Density on the Estimation of Single-Tree Attributes by Hand-Held Mobile Laser Scanning. *Forests* **2019**, *10*, 277. [CrossRef]
31. Hyyppä, E.; Yu, X.; Kaartinen, H.; Hyyppä, J.; Kukko, A.; Holopainen, M.; Vastaranta, M.; Hakala, T.; Karjalainen, M. Comparison of Backpack, Handheld, Under-Canopy UAV, and Above-Canopy UAV Laser Scanning for Field Reference Data Collection in Boreal Forests. *Remote Sens.* **2020**, *12*, 3327. [CrossRef]
32. Stovall, A.E.L.; Vorster, A.G.; Anderson, R.S.; Evangelista, P.H.; Shugart, H.H. Non-Destructive Aboveground Biomass Estimation of Coniferous Trees Using Terrestrial LiDAR. *Remote Sens. Environ.* **2017**, *200*, 31–42. [CrossRef]

Disclaimer/Publisher's Note: The statements, opinions and data contained in all publications are solely those of the individual author(s) and contributor(s) and not of MDPI and/or the editor(s). MDPI and/or the editor(s) disclaim responsibility for any injury to people or property resulting from any ideas, methods, instructions or products referred to in the content.